
Volume 45, 2 February 2012
ISSN 1367-9120
ELSEVIER
Journal of
Asian Earth Sciences
(Formerly the Journal of Southeast Asian Earth Sciences)
Editor-in-Chief
BOR-MING JAHN

Journal of Asian Earth Sciences 45 (2012) 138–149

Contents lists available at SciVerse ScienceDirect

Journal of Asian Earth Sciences

journal homepage: www.elsevier.com/locate/jseaes

Tectonic history of the Irtysh shear zone (NE Kazakhstan): New constraints from zircon U/Pb dating, apatite fission track dating and palaeostress analysis

S. Glorie [a,*], J. De Grave [a], D. Delvaux [b], M.M. Buslov [c], F.I. Zhimulev [c], F. Vanhaecke [d], M.A. Elburg [a], P. Van den haute [a]

[a] MINPET Group, Dept. of Geology & Soil Science, Ghent University, 281-S8 Krijgslaan, 9000 Ghent, Belgium
[b] Dept. of Geology, Royal Museum for Central Africa, 13 Leuvensesteenweg, 3080 Tervuren, Belgium
[c] Institute of Geology & Mineralogy, SB-RAS, 3 prosp. Akad. Koptyuga, 630090 Novosibirsk, Russia
[d] Dept. of Analytical Chemistry, Ghent University, 281-S12 Krijgslaan, 9000 Ghent, Belgium

ARTICLE INFO

Article history:
Received 6 July 2011
Received in revised form 23 September 2011
Accepted 29 September 2011
Available online 20 November 2011

Keywords:
Irtysh shear zone
Central Asian Orogenic Belt
Zircon U/Pb dating
Apatite fission track thermochronology
Palaeostress tensor inversion
Fault kinematics

ABSTRACT

The Irtysh shear zone (ISZ) is an important structure in the framework of the Central Asian Orogenic Belt (CAOB). It represents the site of final collision of Kazakhstan with Siberia during Hercynian times and records up to 1000 km of lateral displacement during subsequent reorganization in the CAOB edifice. We present new zircon U/Pb, apatite fission track and fault kinematic data along the ISZ and consequently derived its tectonic history with emphasis on its formation and reactivation episodes. Carboniferous (~340–320 Ma) zircon U/Pb ages were obtained for the syn- and post-collisional Kalba–Narym intrusives, dating their emplacement in the framework of the Siberia–Kazakhstan collision. During this period, the ISZ experienced an 'early brittle' left-lateral, mainly transtensional stress regime. Late Carboniferous–Early Permian post-collisional intrusives were emplaced and the stress regime changed to a 'late brittle' regime, characterized by more compressional conditions, indicating rheological strengthening as a response to cessation of ductile shearing and cooling of the ISZ crust.

Apatite fission track data and thermal history modeling reveal Late Cretaceous (~100–70 Ma) cooling of the ISZ basement rocks as a response to denudation of a bordering Late Mesozoic Altai orogen. After this denudation event, the tectonic activity ceased during the Late Mesozoic–Early Cenozoic. A final step of cooling (from ~25 Ma), exhibited by some of the thermal history models, may reflect reactivation of the ISZ and initiation of Cenozoic Altai mountain building. The Late Plio-Pleistocene phase of mountain building coincides with a new change in the Palaeostress field, characterized by minor transpressional, right-lateral shear conditions.

1. Introduction and geological setting

The NW-trending Irtysh shear zone (ISZ) (also known as Ertix or Erqis fault) represents a major tectonic boundary between the Siberian and Kazakhstan palaeo-continents in the framework of the Central Asian Orogenic Belt (CAOB) (e.g. Jahn, 2004) or Altaid tectonic collage (Şengör et al., 1993). It can be traced for more than 1000 km from NE Kazakhstan to NW China and might extend even further southwest into Mongolia (Cunningham et al., 1996; Windley et al., 2002; Briggs et al., 2007) (Figs. 1 and 2). The Siberian and Kazakhstan continents converged during the Late Palaeozoic through oblique subduction of the Ob'-Zaysan ocean floor that existed between them. The Ob'-Zaysan ocean is also known as Char or Gobi-Zaysan ocean and represents a part of the Palaeo-Asian Ocean (PAO) (e.g. Buslov et al., 2001; Windley et al., 2007). The Hercynian (late Early Carboniferous) closure of this basin provoked the final amalgamation of the ancestral CAOB (Şengör et al., 1993; Chikov and Zinoviev, 1996; Buslov et al., 2001, 2004; Vladimirov et al., 2003, 2008; Khromykh et al., 2011). This collision occurred along the Char ophiolitic suture-shear zone (CSZ) (Fig. 1) which follows a parallel NW-trend with respect to the ISZ. The CSZ separates the Zharma and Chingiz–Tarbagatai island arcs on one hand from the Rudny-Altai island arc system on the other. These volcanic arcs mark the active margins of the Kazakhstan and Siberian continents respectively. The ISZ separates the Rudny-Altai island arc from the Kalba–Narym fore-arc turbidite complex at the Hercynian active margin of Siberia (Fig. 1) (Buslov et al., 2001, 2004; Vladimirov et al., 2003; Khromykh et al., 2011).

During the Late Carboniferous – Permian, the convergence of Kazakhstan towards Siberia continued and as a consequence, the peri-Gondwanan terrane of Altai-Mongolia was transferred along the edge of Siberia towards the present day Rudny Altai (Fig. 1). The accompanying tectonic forces of oblique subduction

* Corresponding author. Tel.: +32 9 264 4568; fax: +32 9 264 4984.
E-mail address: Stijn.Glorie@UGent.be (S. Glorie).

1367-9120/$ - see front matter © 2011 Elsevier Ltd. All rights reserved.
doi:10.1016/j.jseaes.2011.09.024

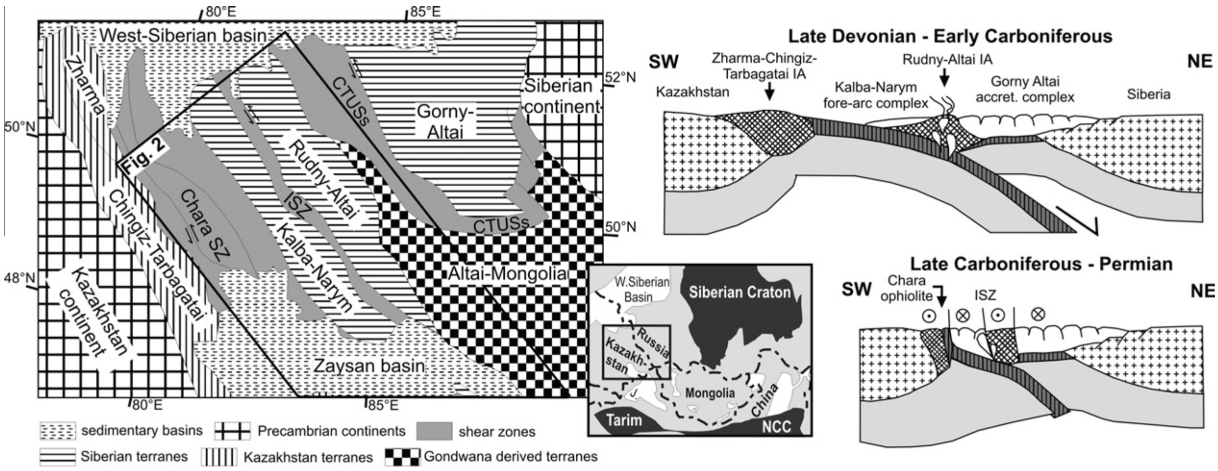

Fig. 1. *Left panel*: Overview of the composing tectonic terranes of the Altai territory and adjacent regions. ISZ = Irtysh shear zone, CTUSs = Charysh Terekta Ulagan Sayan suture, J. = Junggar basin. The Gorny Altai, Rudny Altai and Kalba Narym tectonic units represent island-arc systems and accretionary complexes at the southern margin of the Siberian continent. The Chingiz–Tarbagatai and Zharma–Saur terranes are active margin units of the Kazakhstan continent (after Buslov et al. (2001, 2004). *Right panel*: Schematic SW-NE profiles showing the geodynamic setting of the Altai during the Late Palaeozoic. The Rudny-Altai island arc (IA) and Kalba–Narym fore-arc turbidite complex formed during oblique subduction of the Ob'-Zaysan ocean floor under the Siberian margin. In the Late Carboniferous – Permian, the collision of Siberia and Kazakhstan was completed, initiating strike-slip displacements in the ISZ and other parallel shear zones. See text for more details.

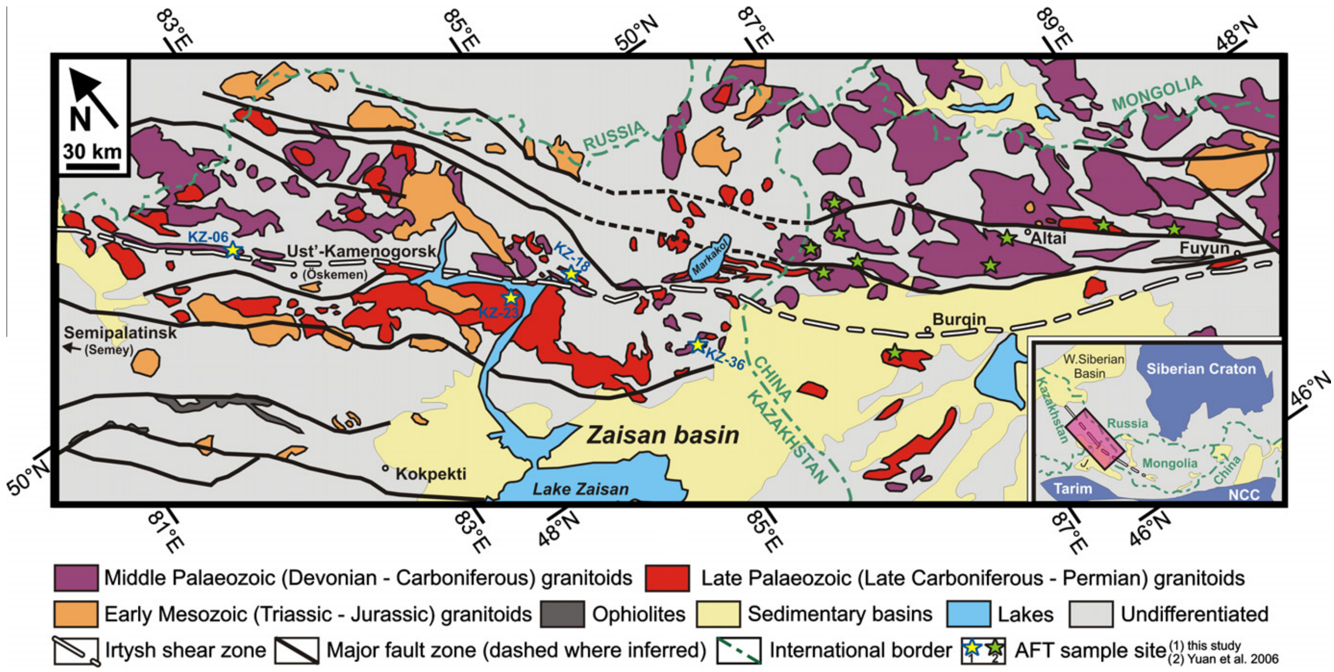

Fig. 2. Simplified geological map of the study area along the Irtysh shear zone. Note that geographical North is at an angle relative to the figure's top. Intrusive complexes are indicated and colour-coded with respect to their inferred emplacement age (based on Vladimirov et al. (2008), Wang et al. (2009) and Chen et al. (2010)). Sample locations for this study are shown by yellow stars on the map. Sample locations from a published apatite fission track study in the Chinese Altai are indicated by green stars (Yuan et al., 2006).

(Ob'-Zaysan) in the West and collision (Altai-Mongolia) in the East (present-day co-ordinates) initiated coeval strike-slip movement along the ISZ and CSZ. Multi-mineral $^{40}Ar/^{39}Ar$ ages record two major stages of left-lateral deformation in the ISZ at ~285–270 Ma and ~270–260 Ma (Travin et al., 2001). It is thought that both the ISZ and CSZ accommodated more than 1000 km sinistral strike-slip displacement during this period of time (Melnikov et al., 1997; Burtman et al., 1998; Buslov et al., 2004; Vladimirov et al., 2008). The Rudny-Altai granitoids (NE of the ISZ) mainly have Devonian – Early Carboniferous crystallization ages (Fig. 2). They were emplaced during subduction and closure of the Ob'-Zaisan ocean and the collision of Siberia with Kazakhstan and Junggar. South of the ISZ, in the Kalba–Narym terrane, granitoids yield younger, Late Carboniferous – Permian ages, coinciding with the timing of major displacement along the ISZ (Fig. 2). Hence, the Kalba–Narym intrusions are thought to be emplaced in a post-collisional setting associated with ISZ activity (Vladimirov et al., 2001, 2008). The granitoids associated with the ISZ are deformed and show a ductile mylonitic fabric, indicating that the ISZ remained active after their emplacement (Chikov and Zinoviev, 1996; Melnikov et al., 1997; Buslov et al., 2004; Pirajno, 2010). Early Mesozoic (Triassic–Jurassic) granitoids are found at both sides of the ISZ (Fig. 2) and were emplaced in an intra-plate setting, possibly related to the supposed Tarim plume activity (Vladimirov et al., 2001; Chikov et al., 2008; Pirajno, 2010).

The present mountainous morphology of the Altai is thought to have formed during reactivation of inherited structures such as Late Palaeozoic faults, of which the ISZ is a prime example (Allen and Vincent, 1997; Yuan et al., 2006; Briggs et al., 2007; Buslov, 2011). As a response to ongoing left-lateral displacements during the Late Permian–Early Triassic, the Junggar basin opened as a large intracontinental pull-apart basin along the southern edge of the ISZ (Allen et al., 1995). The Zaysan basin in fact forms the northwestern part of the Junggar basin at the Kazakh–Chinese border (Figs. 1 and 2) and received up to 6 km of Mesozoic and Cenozoic clastic sediments, derived from the adjacent eroding Altai orogen (Thomas et al., 2002). Sedimentation in the Zaysan basin was almost continuous from the Triassic until the Early Neogene, with a major interruption between the Middle Jurassic and the Late Cretaceous (Delvaux et al., 1996). During the Late Neogene (Plio-Pleistocene), tectonic activity increased, giving rise to the Cenozoic Altai orogen as it appears today. This renewed reactivation phase is generally interpreted as a far-field effect of the India-Eurasia collision (De Grave and Van den haute, 2002; De Grave et al., 2007).

Although the general geodynamic evolution of the ISZ and its bordering terranes is known, absolute radiometric age information on these tectonic episodes is limited and the fault kinematics of the ISZ are poorly understood. A comprehensive zircon U/Pb dataset exists for both the Kazakh and Chinese segments of the ISZ (e.g. Vladimirov et al., 2001, 2008; Wang et al., 2009 and references therein; Chen et al., 2010), but such data are lacking for the granitoids in the intervening border zone. Furthermore, thermochronological studies, which date basement cooling as a response to various tectonic events (e.g. Reiners and Ehlers, 2005), were performed exclusively along the Chinese ISZ segment (Yuan et al., 2006, 2009) and are non-existent for the Kazakh part (Fig. 2). In this work, we present new zircon U/Pb and thermochronological (apatite fission track) data along the Kazakh ISZ, in order to enhance our understanding of the tectonic evolution of this key-region within the CAOB. In addition, the ISZ fault kinematics were investigated based on palaeostress tensor inversion with special attention to the timing of tectonic movements. Combining all these data and with additional support of existing $^{40}Ar/^{39}Ar$ ages, we are now able to reconstruct the thermotectonic history of the ISZ from the time of its formation until its final reactivation, creating the present NE Kazakh Rudny-Altai mountains.

2. Sample locations and methodology

2.1. Zircon LA-IC-MS U/Pb dating

Two granitic intrusions in the Kalba–Narym terrane were sampled for zircon U/Pb (ZUPb) analysis. Sample KZ-23 comes from the main Kalba–Narym batholith at the shores of the Buktharma artificial lake (a branch of Lake Zaysan), while KZ-36 was sampled in a small granitic pluton from the Kaldjir plateau, close to the Kazakh–Chinese border (Table 1, Fig. 2). Zircon separates were embedded and polished for LA-ICP-(SF)-MS (Laser Ablation-Inductively Coupled Plasma-(Sector Field)-Mass Spectrometry) U/Pb (ZUPb) dating. Using this technique, the zircon crystallization ages (closure-T ~800–1000 °C) of the sampled intrusives were determined in order to constrain the timing of pluton emplacement (Cherniak and Watson, 2003). The U/Pb analyses were carried out at the LA-ICP-(SF)-MS facility of the Department of Analytical Chemistry at Ghent University, using identical analytical procedures as those described in Glorie et al. (2011b) and De Grave et al. (2011). The internal structure of the zircon crystals was investigated and mapped by cathodoluminescence (CL) imaging, using a JEOL JSM-6400 SEM (Scanning Electron Microscope). Reference zircon GJ-1 (Jackson et al., 2004) was used as primary standard and Plešovice zircon (Sláma et al., 2008) for validation purposes (Glorie et al., 2011b). Data reduction was performed using the PepiAGE-software (Dunkl et al., 2009) and the age results were plotted on a Wetherill concordia diagram using the Isoplot program (Ludwig, 2003).

2.2. Apatite fission track thermochronology

In order to reconstruct the post-emplacement thermal history, four basement apatite samples were analyzed using the apatite fission track (AFT) method (Wagner and Van den haute, 1992). The resulting AFT ages are cooling ages that can be linked to movements in the upper crust corresponding to exhumation and denudation of the sampled intrusions (e.g. De Grave and Van den haute, 2002; Glorie et al., 2010; De Grave et al., 2011; Jolivet et al., 2011). In this study, we followed the analytical procedures described by De Grave et al. (2011) and Glorie et al. (2011a). KZ-06 and KZ-18 were sampled in sheared granitoids along the ISZ (Table 1, Fig. 2). KZ-23 and KZ-36 come from the Kalba–Narym batholith and as mentioned were also analyzed with the ZUPb dating method. Spontaneous fission tracks in apatite were etched with a 2.5% HNO_3 solution for 70 s at 25 °C, induced tracks in mica with 40% HF for 40 min at 20 °C. Irradiation was carried out in the Belgian Reactor 1 (BR1) facility of the Belgian Nuclear Research Centre in Mol (channel X26), with a thermal neutron fluence of 2.17×10^{15} cm^{-2}. Both Q-ages (based on the calculated absolute thermal neutron fluence) and conventional ζ-ages (calibration factor based on IRMM 540 dosimeter glass) were calculated.

AFT lengths were measured on horizontal confined fission tracks using an identical experimental setup as described in Glorie et al. (2010). Where possible 100 natural confined tracks were measured to construct an AFT length-frequency distribution, a number that was not always attained. Subsequent AFT thermal history modeling was carried out using the HeFTy software (Ketcham, 2005) using identical settings as in Glorie et al. (2010) and Glorie et al. (2011a). One time–Temperature (tT)-constraint was introduced, reflecting the apparent AFT age of the sample. More geological constraints were not available to aid the modeling process. D_{par} (Donelick et al., 1999) values were found to be identical to the obtained values for Durango apatite (~1.5–1.9 μm) in our laboratory conditions and therefore a fixed l_0 parameter of 15.95 μm was used for the initial AFT length (Glorie et al., 2010, 2011a).

2.3. Stress inversion of fault-slip data

Fault-slip measurements were performed in several sites along the ISZ to reconstruct Palaeostress tensors with the program Win_Tensor (Delvaux, 2011). The same procedure was used as

Table 1
List of sample locations along the ISZ.

Sample	Latitude	Longitude	Alt. (m)	Locality	Lithology
KZ-06	N49°53′29″	E082°37′49″	340	Irtysh SZ, near Ust'-Kamenogorsk	Granite-gneiss
KZ-18	N49°06′22″	E084°33′34″	1500	Irtysh SZ, near Kok-Terek village	Granodiorite
KZ-23	N49°14′29″	E084°08′30″	580	Kalba–Narym, near lake Bukhtarma	Granite
KZ-36	N48°16′26″	E085°01′18″	1100	Kaldjir plateau	Granite

described by Delvaux and Sperner (2003). Stress inversion allows to reconstruct the four main parameters of the reduced tectonic stress tensor (Wallace, 1951; Bott, 1959; Angelier, 1989, 1994): the orientation of the three orthogonal principal stress axes: σ_1, σ_2 and σ_3 (with $\sigma_1 \geqslant \sigma_2 \geqslant \sigma_3$) and the stress ratio $R = (\sigma_2 - \sigma_3)/(\sigma_1 - \sigma_3)$ which expresses the magnitude of σ_2 relative to σ_1 and σ_3. These four parameters were determined using an iterative rotational stress tensor optimalization procedure, which jointly minimizes the slip deviation between the observed slip lines and the resolved shear stress. It furthermore favours slip on the fault planes by minimizing the resolved normal stress magnitude and maximizing the resolved shear stress magnitude. Using the four parameters of the reduced stress tensor, the horizontal principal stress S_{Hmax}/S_{Hmin} was computed following the method of Lund and Townend (2007) and a stress regime index R' was determined. The latter forms a continuous scale from 0 (radial extension) to 3 (constriction) and ranges from 0 to 1 for normal faulting regimes, from 1 to 2 for strike-slip regimes and from 2 to 3 for thrust faulting regimes (Delvaux et al., 1997; Delvaux and Sperner, 2003). The uncertainties in the determination of the stress axes and stress ratio R were used to determine the 1σ standard deviation for S_{Hmax}/S_{Hmin} and R'.

3. Results

3.1. Zircon LA-ICP-MS U/Pb dating

The obtained ZUPb data are summarized in Table 2, listing the results for each analyzed zircon crystal (excluding common-Pb polluted analyses; <10% for both samples). Concordia plots are presented in Fig. 3 and the resulting ZUPb ages are compared with published data in Fig. 4 (discussed further in Section 4.1). Sample KZ-36 yields within error identical (common Pb-corrected) $^{206}Pb/^{238}U$ and $^{207}Pb/^{235}U$ results for all analyzed grains, defining a U/Pb concordia age of 338 ± 5 Ma (Fig. 3). This Early Carboniferous (Visean) age is interpreted to represent the time of crystallization of the Kaldjir granitoids at the northern margins of the Zaysan basin. For sample KZ-23, $^{206}Pb/^{238}U$ and $^{207}Pb/^{235}U$ ages range from ~300 to 1125 Ma, defining a discordia line in the Wetherill concordia diagram. This discordia exhibits an upper intercept of 1187 ± 83 Ma and lower intercept of 310 ± 36 Ma with the concordia curve. Ten out of seventeen analyses cluster around the lower intercept, defining a concordia age of 320 ± 5 Ma (Fig. 3). This late Early Carboniferous (Serpukhovian–Bashkirian transition) age is interpreted to represent the time of the emplacement of the Kalba–Narym intrusion. The older, Meso-Proterozoic ages probably represent partially retained inherited ZUPb ages (discussed further).

3.2. Apatite fission track dating and thermal history models

AFT results are presented in Table 3. For all samples, within error identical Late Cretaceous ζ- and Q-AFT ages were obtained. The oldest ages fall at the boundary between the Early and Late Cretaceous. Interestingly, samples KZ-06 (87 ± 6 Ma) and especially KZ-18 (71 ± 4 Ma) from within the ISZ yield a slightly younger AFT age than the samples from the bordering Kalba–Narym intrusions (KZ-23 and KZ-36). The latter samples yield AFT ages of 95 ± 5 Ma and

Table 2
Zircon LA-ICP-MS U/Pb (ZUPb) results.

	n°	^{207}Pb[a] (cps)	U[b] (ppm)	Pb[b] (ppm)	$\frac{Th}{U}$[b]	$\frac{^{206}Pb}{^{204}Pb}$	$\frac{^{206}Pb}{^{238}U}$[c]	±2σ (%)	$\frac{^{207}Pb}{^{235}U}$[c]	±2σ (%)	$\frac{^{207}Pb}{^{206}Pb}$[c]	±2σ (%)	rho[d]	$\frac{^{206}Pb}{^{238}U}$[e]	±2σ (Ma)	$\frac{^{207}Pb}{^{235}U}$[e]	±2σ (Ma)	Con.[f]
KZ-23	1	6919	370	41	0.79	700	0.1109	8.8	1.0920	9.6	0.0714	3.9	0.92	678	57	749	52	111
	2	2007	213	14	0.60	1189	0.0610	2.9	0.4706	4.6	0.0559	3.6	0.63	382	11	392	15	103
	3	24,469	972	122	0.04	18,809	0.1339	5.4	1.3034	5.6	0.0679	2.3	0.96	810	41	847	33	105
	4	4664	601	32	0.75	1692	0.0517	6.6	0.4224	10.1	0.0593	7.6	0.65	325	21	358	31	110
	5	16,863	995	83	0.78	1562	0.0833	8.6	0.8480	10.9	0.0739	6.7	0.79	515	43	624	52	121
	6	7707	1037	58	0.66	2776	0.0507	2.3	0.3813	3.6	0.0546	2.7	0.66	319	7	328	10	103
	7	812	96	5	0.53	197	0.0525	4.2	0.4173	9.4	0.0576	8.4	0.45	330	14	354	29	107
	8	3358	305	25	0.81	11,913	0.0736	4.6	0.6376	5.1	0.0559	3.4	0.90	458	20	501	20	109
	9	14,571	368	76	0.68	1131	0.1827	6.3	2.0229	9.4	0.0843	6.4	0.67	1082	63	1123	66	104
	10	12,660	1536	86	0.13	74,402	0.0583	4.7	0.4612	5.6	0.0574	3.1	0.84	365	17	385	18	105
	11	756	102	5	0.37	310	0.0503	3.9	0.3890	10.0	0.0561	9.2	0.39	316	12	334	29	105
	12	1134	162	9	0.34	1500	0.0548	9.2	0.3941	13.1	0.0522	9.3	0.71	344	31	337	38	98
	13	456	71	4	0.49	351	0.0501	3.1	0.3515	11.1	0.0509	10.7	0.27	315	9	306	30	97
	14	836	116	6	0.42	224	0.0522	3.5	0.3853	9.7	0.0536	9.0	0.37	328	11	331	28	101
	15	586	81	4	0.42	250	0.0482	4.3	0.3997	11.3	0.0601	10.5	0.38	304	13	341	33	112
	16	775	118	6	0.56	521	0.0503	2.9	0.3555	7.1	0.0513	6.5	0.41	316	9	309	19	98
	17	1148	169	10	0.67	335	0.0525	3.2	0.3764	7.9	0.0520	7.2	0.41	330	10	324	22	98
KZ-36	1	1730	189	11	0.37	3987	0.0547	3.1	0.3975	8.4	0.0527	7.8	0.37	343	11	340	25	99
	2	1553	166	9	0.34	2416	0.0523	3.5	0.4082	9.2	0.0566	8.5	0.38	329	11	348	28	106
	3	2963	345	18	0.27	53,761	0.0540	6.1	0.4268	10.9	0.0573	9.0	0.56	339	20	361	34	106
	4	3670	420	25	0.51	865	0.0565	4.4	0.4320	6.7	0.0554	5.0	0.66	355	15	365	21	103
	5	4156	486	28	0.59	1131	0.0545	3.2	0.3904	4.8	0.0520	3.5	0.67	342	11	335	14	98
	6	10,545	1330	73	0.36	9832	0.0536	5.6	0.4014	7.1	0.0543	4.4	0.79	337	18	343	21	102
	7	4837	580	34	0.46	2402	0.0564	3.5	0.4060	4.7	0.0522	3.2	0.74	354	12	346	14	98
	8	3320	391	23	0.49	6241	0.0555	2.9	0.4045	4.5	0.0529	3.5	0.63	348	10	345	13	99
	9	4706	584	30	0.37	1339	0.0515	3.0	0.3851	5.3	0.0542	4.3	0.57	324	10	331	15	102
	10	9113	1149	64	0.47	6174	0.0536	3.7	0.3941	5.1	0.0534	3.5	0.73	336	12	337	15	100
	11	910	116	6	0.32	435	0.0523	3.3	0.3754	9.3	0.0520	8.7	0.35	329	10	324	26	98
	12	984	120	6	0.27	654	0.0532	3.1	0.4085	7.2	0.0557	6.5	0.43	334	10	348	21	104

[a] Within-run, background-corrected mean ^{207}Pb signal.
[b] U and Pb content and Th/U ratio were calculated relative to the GJ-1 zircon standard.
[c] Corrected for: background, within-run Pb/U fractionation ($^{206}Pb/^{238}U$), common Pb and normalised to GJ-1 reference standard.
[d] Rho is the error correlation defined as err$^{206}Pb/^{238}U$/err$^{207}Pb/^{235}U$.
[e] U/Pb ages were calculated with Isoplot (Ludwig, 2003).
[f] Degree of concordance = age$^{206}Pb/^{238}U$/age$^{207}Pb/^{206}Pb \times 100$.

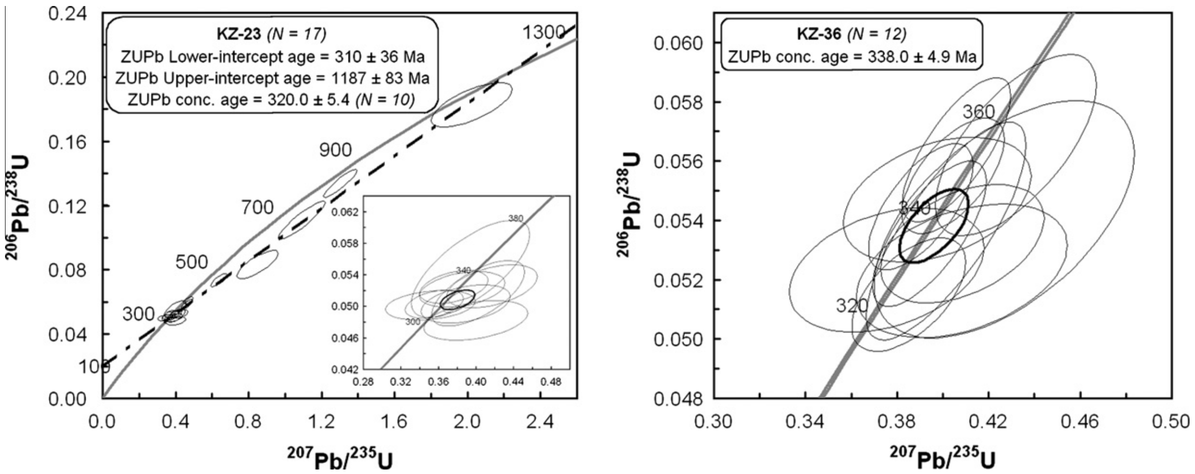

Fig. 3. Zircon $^{206}Pb/^{238}U$ versus $^{207}Pb/^{235}U$ concordia plots. All data-point error ellipses were calculated at the 2σ level. Concordant ages are indicated by the central bold ellipses. Discordant ages (KZ-23) are arranged along a discordia line (bold dashed) and define upper- and lower-intercept ages with the concordia.

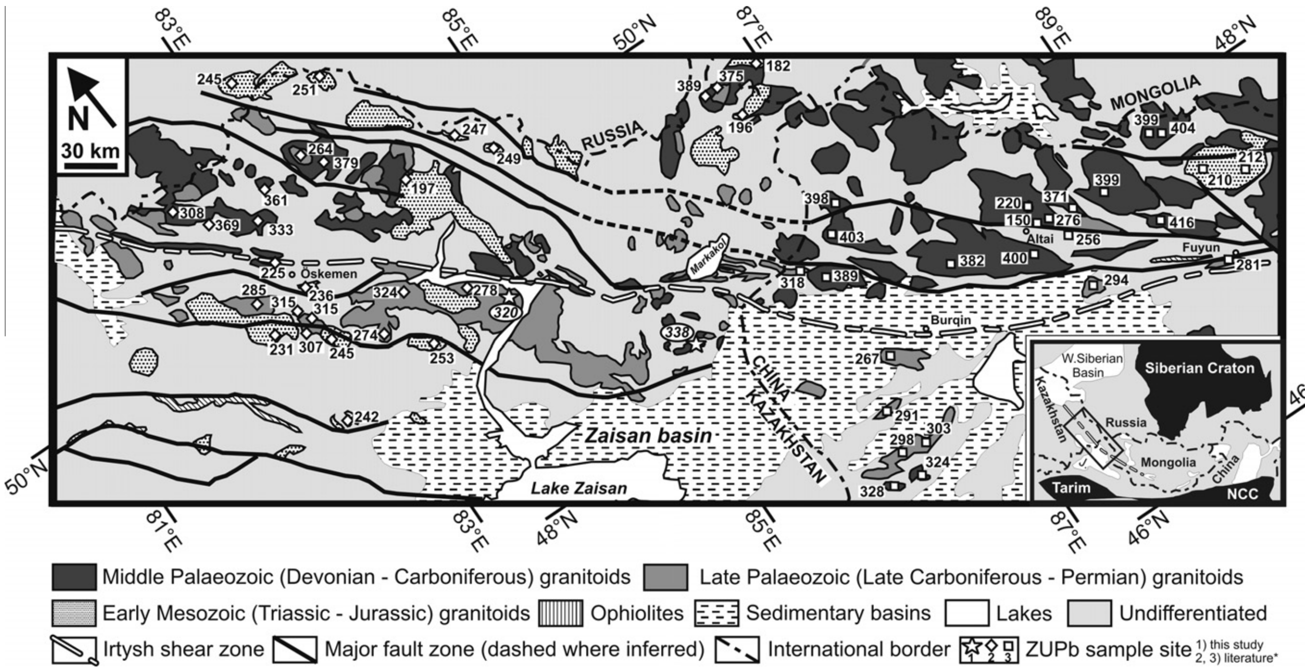

Fig. 4. Compilation of published zircon U/Pb data along the ISZ in the Kazakh and Chinese Altai. Star symbols refer to our new ages. Diamonds refer to published ZUPb studies in the Kazakh Altai (Vladimirov et al., 2001; Kuibida et al., 2009; Dokukina et al., 2010; Pirajno, 2010), squares to ZUPb studies in the Chinese Altai (Yuan et al., 2007; Wang et al., 2009; Chen et al., 2010 and references therein).

Table 3
Apatite fission track (AFT) results.

Sample	n[a]	ρ_s (±1σ)[b]	N_s[c]	ρ_i (±1σ)[b]	N_i[c]	ρ_d (±1σ)[b]	N_d[c]	ρ_s/ρ_i	$P(\chi^2)$[d]	$t(\zeta)$[e]	$t(Q)$[e]	l_m[f]	n_l[f]	σ[f]
Apatite fission track (AFT) results														
KZ-06	60	2.431 (0.096)	636	1.546 (0.076)	409	4.272 (0.105)	1640	1.589 ± 0.101	1.00	87.4 ± 6.0	87.6 ± 6.1	–	–	–
KZ-18	25	12.846 (0.374)	1183	10.050 (0.332)	918	4.269 (0.105)	1639	1.299 ± 0.057	0.61	71.4 ± 3.7	71.6 ± 3.7	13.4	76	1.1
KZ-23	30	13.128 (0.276)	2263	7.647 (0.211)	1318	4.268 (0.105)	1639	1.722 ± 0.060	0.98	94.5 ± 4.2	94.7 ± 4.2	13.5	100	1.3
KZ-36	40	5.800 (0.162)	1276	3.248 (0.121)	716	4.265 (0.105)	1638	1.813 ± 0.085	0.99	99.4 ± 5.4	99.6 ± 5.4	13.4	100	1.4

[a] n is the number of analyzed grains.
[b] ρ_s, ρ_i, and ρ_d are the density of spontaneous, induced tracks and induced tracks in an external detector (ED) irradiated against a dosimeter glass (IRMM-540). ρ_s, ρ_i and ρ_d are expressed as 10^5 tracks/cm^2.
[c] N_s, N_i, and N_d are the number of counted spontaneous, induced tracks and induced tracks in the ED (N_d is an interpolated value).
[d] $P(\chi^2)$ is the chi-squared probability that the dated grains have a constant ρ_s/ρ_i-ratio.
[e] $t(\zeta)$ and $t(Q)$ give the resulting ages, expressed in Ma.
[f] AFT length data are reported as a mean track length (l_m) with standard deviation σ (in μm), obtained from the measurement of a number (n_l) of natural, horizontal confined tracks. See text for more details.

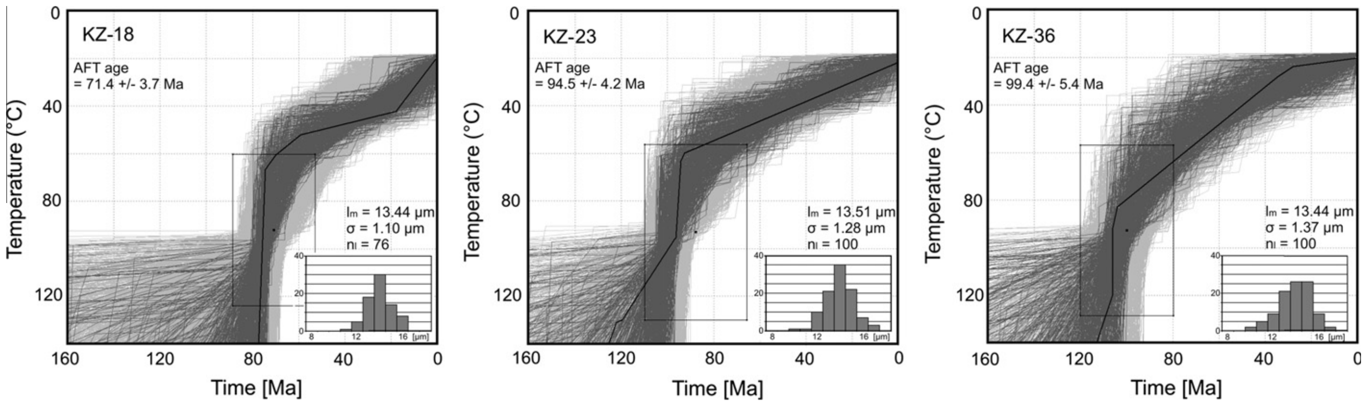

Fig. 5. Resulting thermal history models based on the AFT (apatite fission track) age and length data. Time–temperature box constraints were placed at the AFT age only. AFT length frequency distributions are shown in each plot: l_m = the mean AFT length with its 1σ standard deviation, n_l = number of measured horizontal confined tracks. The models for samples KZ-23 and KZ-36 record fast cooling at ~110–95 Ma to ~80–60 °C, followed by slow cooling from ~100–85 Ma to ambient temperatures. The thermal history model for KZ-18 exhibits a 3-step cooling curve, with fast cooling at ~85–75 Ma to ~60 °C, followed by slow cooling until ~40 °C and apparent increased cooling from ~25 Ma onwards.

100 ± 4 Ma, respectively (Table 3). For three samples, a sufficient number of confined fission tracks could be measured to obtain relevant AFT length frequency distributions. These distributions exhibit a mean track length of 13.4–13.5 µm, are relatively narrow (σ = 1.1–1.4 µm) and slightly negatively skewed (Fig. 5).

Subsequent modeling of the AFT data reveals a similar thermal history model for samples KZ-23 and KZ-36, showing (1) fast cooling at ~110–95 Ma to ~80–60 °C followed by (2) slow cooling from ~100–85 Ma to ambient temperatures. The thermal history model for KZ-18 exhibits a slightly different, 3-step cooling curve, with (1) fast cooling at ~85–75 Ma to ~60 °C followed by (2) slow cooling until ~40 °C and (3) a final phase of fast cooling from ~25 Ma onwards (Fig. 5).

3.3. Fault kinematics and stress inversion results

The ductile and brittle kinematic data have been measured at 11 sites or site-groups near Ust-Kamenogorsk (sites KZ-01-10 in the ISZ and KZ-11 in the Kalba–Narym granitoids), around the Bukhtarma artifical lake (sites KZ-13-16 and KZ-21-22 in the Kalba–Narym granitoids) and in the Narym range (sites KZ-17-20 in Rudny-Altai island arc associated rocks) (Table 4, Fig. 6). The ductile shear fabric of the ISZ is characterized by a WNW-trending subvertical mylonitic foliation, including subhorizontal mineral lineations and sheath fold axes. Furthermore, consistent indicators for left-lateral displacement were recognized (Figs. 7 and 8). The Bukhtarma granitoids are often massive, but may contain subvertical tectonic and/or magmatic NW-trending foliation (Fig. 7, KZ-13-23). Mylonitic foliation with shear sense indicators are not observed along the shore of the artificial lake, but it may be present along the central part of the shear zone.

Most of the brittle fault-slip data seem to be related to the ISZ, and are attributed to the brittle-ductile transition zone or later movements. The brittle faults that affect the ductile fabric of the ISZ are related to later brittle movements that crosscut the mylonitic foliation obliquely (Sites KZ-01-09). The Kalba–Narym granitoids contain numerous and well-expressed fracture planes, often affected by chlorite-epidote alteration. They can occur as large conjugated fracture systems (Sites KZ-11, -13, -14), or in tectonic breccias which are cemented by quartz and chlorite-epidote (Sites KZ-21-22). In the Narym range and in two sites along the Bukhtarma lake (Sites KZ-14, 21) (Fig. 6), faults with a markedly different aspect of unconsolidated breccias were detected, which were in some cases coated with iron oxide. These faults reflect a younger right-lateral reactivation of the ISZ along the Bukhtarma lake, and correspond to thrust movements in the Narym range.

The stress tensors were separated into three palaeostress stages (Figs. 7 and 8), based on the field settings, crosscutting relationships and fault-rock characteristics as summarized above. The first stage (four tensors, 86 fractures, 49 slip lines) corresponds to an average E–W S_{Hmax} in a strike-slip regime (R' = 1.4), with three tensors showing transtension and one transpression. The second stage (eight stress tensors, 154 fractures, 125 slip lines) exhibits a ENE-WSW S_{Hmax} in an average strike-slip to transpressional context (R' = 1.73) with individual transtensional to pure compressional stress regimes. The third stage yields a more compressional (average R' = 2.03) signature with a nearly N–S S_{Hmax}.

4. Interpretation and discussion

4.1. Ob'-Zaysan closure and Irtysh shear zone formation: Late Palaeozoic granitoids

A compilation of published zircon U/Pb ages for intrusives in the terranes bordering the ISZ (in both the Kazakh and Chinese segments) is presented in Fig. 4. Ob'-Zaysan subduction related intrusives are found in the NE of the ISZ (in the Rudny Altai and southern Altai-Mongolia terrane), yielding Devonian – Early Carboniferous emplacement ages (~410–330 Ma) with the oldest in the East (in the Chinese segment) (Vladimirov et al., 2001; Wang et al., 2009 and references therein). This observation is in agreement with the oblique subduction model of Ob'-Zaysan oceanic crust under the Kazakhstan continent from the SE to the NW (present-day co-ordintates) (e.g. Buslov et al., 2001; Yuan et al., 2007; Vladimirov et al., 2008). South of the ISZ, the intrusives in the Kalba–Narym terrane and in the Chinese Saur mountains have consistent Late Carboniferous–Early Permian ages (~330–275 Ma) and are interpreted as post-collisional plutons (Vladimirov et al., 2001; Chen et al., 2010 and references therein). Our ZUPb samples were taken in the Kalba Narym terrane and yield emplacement ages of ~338 Ma and ~320 Ma. These late Early Carboniferous ages are not unexpected, given their location close to the junction zone between the magmatic domains north and south of the ISZ. Therefore we interpret our ZUPb results in the context of the final collision of Siberia and Kazakhstan. As mentioned earlier, the initiation of ISZ shear is dated to the Late Palaeozoic (~285–260 Ma) by multi-mineral $^{40}Ar/^{39}Ar$ data (Travin et al., 2001).

Table 4
Stress inversion results. *N*: number of fault and fracture data used for the stress tensor calculation, Nt: total number of measured data in the original set, σ_1, σ_2, σ_3: stress axis (pl: plunge angle, az: azimuth), R: stress ratio $(\sigma_2 - \sigma_3)/(\sigma_1 - \sigma_3)$, S_H: horizontal principal stress directions with S_{Hmax} for compression, S_{Hmin} for extension and 1σ standard deviation. Stress Regime with stress regime index R' (0–1 for normal faulting, 1–2 for strike-slip faulting and 2–3 for thrust-faulting regimes), 1σ standard deviation for R' and regime qualification as in the World Stress Map (UF: oblique faulting, SS: strike-slip, TF: thrust faulting), QR: quality rank estimation according to the World Stress Map (A: excellent, B: good, C: medium, D: poor).

Site ID	Location			Fault-rock		Data		σ_1		σ_2		σ_3		*R*	S_H			Regime			Qual.
Ref.	Long	Lat	Name	Host rock	Structure	N	Nt	pl	az	pl	az	pl	az		Max	Min	1σ	R'	1σ	Reg	QR
KZ-01-02	82.277	50.209	Ust-Kamenogorsk	ISZ granitoids	Mylonitic foliation	13															
					Conjugated fractures	14	25	07	243	15	335	74	129	0.02	063	153	3.1	2.02	0.09	TF	C
KZ-05-08	82.320	50.224	Ust-Kamenogorsk	ISZ granitoids	Mylonitic foliation	13															
					Faults and fractures	14	29	30	054	59	218	07	320	0.35	051	141	8.5	1.65	0.26	SS	D
KZ-09	82.264	50.254	Ust-Kamenogorsk	Granitic gneiss	Mylonitic foliation	19															
				lense in ISZ	Brittle faults	9	30	16	221	74	050	02	311	0.82	041	131	6.2	1.18	0.45	SS	D
KZ-11	82.111	50.035	Ust-Kamenogorsk	K-N granites	Large fracture systems	35	33	35	243	51	094	15	344	0.91	073	163	7.5	1.09	0.42	SS	C
KZ-13-23	84.131	49.258	Bukhtarma, camp site	K-N granites	Magmatic & mylonitic foliation	17															
					Faults with chlorite–epidote	35	103	20	285	61	059	19	188	0.87	099	009	5.7	1.13	0.13	SS	C
					Brittle faults	51	103	22	064	68	242	00	334	0.88	064	154	10.5	1.12	0.46	SS	B
KZ-14	84.112	49.254	Bukhtarma, pontoon	K-N granites	Large strike-slip faults	34	73	17	045	68	267	15	139	0.58	048	138	8.9	1.42	0.43	SS	B
					Late movements along lake shore	20	73	12	167	72	299	13	074	0.22	166	076	3	1.78	0.28	SS	D
KZ-15	83.907	49.465	Bukhtarma, right bank	Andesite	Brittle faults	7	8	10	064	49	322	39	163	0.54	068	158	5.8	1.46	0.23	SS	D
KZ-16	83.981	49.393	Bukhtarma, right bank	K-N granites	Faults with clorite-epidote	11	14	28	230	23	127	52	004	0.43	059	149	19.2	2.43	0.35	UF	C
KZ-17-20	84.511	49.116	Narym range	Volcano-clastics	Recent thrust faulting	31	35	08	335	76	097	12	243	0.08	154	064	3.6	1.92	0.12	SS	C
KZ-21	83.983	49.395	Bukhtarma, right bank	Granodiorite	Tectonic breccia with quartz-	9	59	06	287	38	022	51	190	0.33	106	016	9.4	2.33	0.23	TS	D
					chlorite-epidote	28	54	27	246	06	154	63	053	0.55	072	162	15.1	2.55	0.18	TF	C
					Late large planes with iron-oxide	14	54	27	360	01	268	63	176	0.4	180	090	3.2	2.4	0.1	TF	D
KZ-22	83.985	49.397	Bukhtarma, right bank	Granodiorite	Tectonic breccia with chlorite-epidote	18	30	17	102	70	246	11	009	0.85	099	009	7.9	1.15	0.28	SS	C

The origin of the older zircons in sample KZ-23, at the junction zone between the Kazakhstan and Siberian active margin terranes, is debatable. Their lower intercept age coincides with the concordant age for the other zircons, suggesting that the inherited zircons were partially reset during the Kalba–Narym granitoid magma generation. Given the observation that the inherited zircons define a single Meso-Proterozoic upper intercept with the concordia curve, we argue that this upper intercept age may represent the original age of an igneous protolith. An alternative theory could be that the older zircons represent exotic zircons which were incorporated in the granitoid magma during its ascent in the crust. It is however less likely that the (metasedimentary) country rock zircons yield a homogeneous U/Pb age population. Additional petrological and/or geochemical data are however necessary to determine more precisely the origin of the older zircons.

Meso-Proterozoic ages were found at the Altai-Mongolia margin in the Charysh–Terekta–Ulagan–Sayan suture-shear zone (CTUSs; Fig. 1) and are thought to be related to ancient events in the context of the Palaeo-Kazakhstan assembly (Glorie et al., 2011b). They also appear in other microcontinental terranes within the Palaeo-Kazakhstan edifice: e.g. the Tuva-Mongolia and Southern Gobi microcontinents (Kozakov et al., 1999; Demoux et al., 2009). North of the CTUSs, in Gorny Altai, no Meso-Proterozoic ages are found at all (Glorie et al., 2011b), which indicates that the older zircons are probably related to the Kazakhstan continent, rather than to the Siberian continent.

Vladimirov et al. (2001, 2008) discussed four intrusion phases in the Kalba–Narym batholith with ZUPb ages of 307–299 Ma for the Kunush plagiogranite complex, 295–274 Ma for the Early Kalba complex, 253–245 Ma for the Late Kalba complex and 231–225 Ma for the Monastyr complex. Our results for sample KZ-23 (~320 Ma) indicate that Kalba–Narym magmatism may have started already earlier. The youngest Late Permian–Early Mesozoic crystallization ages occur throughout the entire study area and are also found further north in Gorny Altai and in the basement underneath the West Siberian basin (Vladimirov et al., 2001; Wang et al., 2009; Pirajno, 2010; Glorie et al., 2011b). These emplacement ages are interpreted to reflect intraplate magmatism, possibly related to the Siberian and/or Tarim plume activity (e.g. Vladimirov et al., 2008; Pirajno, 2010). This plume activity hypothesis however remains controversial. Alternatively, a model of slab break-off was proposed for the origin of the Late Permian - Triassic granitoids, suggesting that they are derived from mantle wedges that were metasomatised by earlier subducting crust and magmatic arcs in the CAOB framework (e.g. Yuan et al., 2010; Glorie et al., 2011b).

4.2. Meso-Cenozoic reactivation

The Late Cretaceous AFT cooling ages, obtained in this study confirm earlier reported results in the Altai territory (De Grave and Van den haute, 2002; Yuan et al., 2006; Jolivet et al., 2007; Vassallo et al., 2007; De Grave et al., 2008, 2009). While Yuan et al. (2006) published ~30 AFT ages for the Chinese Altai, just North of the ISZ (Fig. 2), we report the first AFT data obtained for the Kazakh (Rudny) Altai. Our AFT ages range between ~100 and 70 Ma, which corroborates the Chinese Altai AFT data very well. The thermal history models show that these ages do not represent mixing ages between younger and older events, but give evidence of an episode of fast cooling in the (early) Late Cretaceous. We interpret this cooling event as the result of increased uplift and denudation of a Mesozoic Altai orogen. Various signs of Cretaceous regional compression and fault reactivation in the Junggar basin bear witness to tectonic deformation of the Cental Asian crust at that time (Allen and Vincent, 1997; Vincent and Allen, 2001; Chikov et al., 2008). The AFT signal also coincides with a major stratigraphic hiatus between the Middle Jurassic and the Late

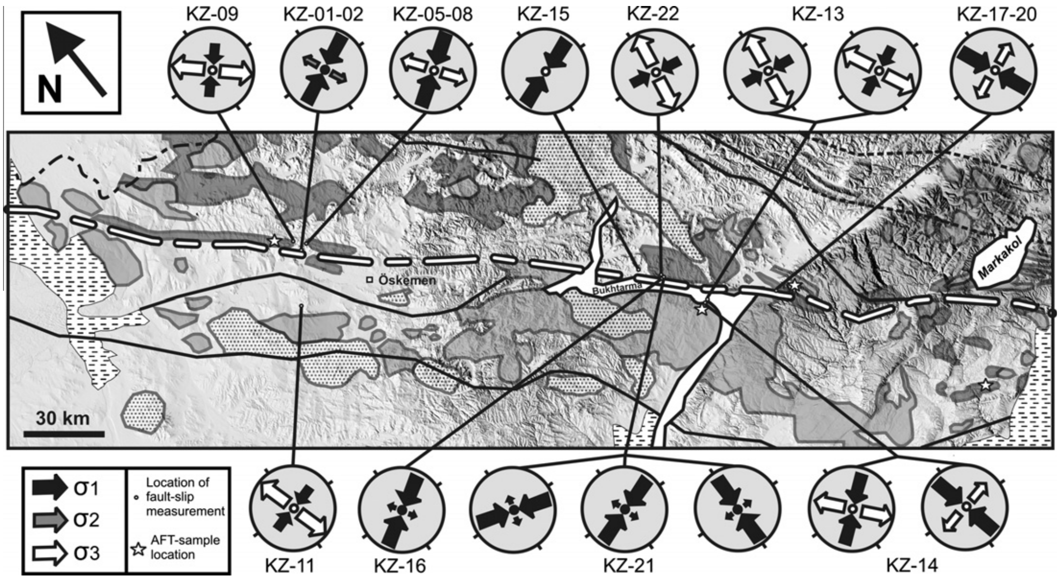

Fig. 6. Digital terrain model with indication of our obtained stress tensor data along the ISZ. Map key as in Fig. 4 and stress tensor diagrams as in Fig. 7 (oriented according to the inclined geographical north on the map).

Cretaceous strata in the Zaysan basin (Delvaux et al., 1996). The driving forces that established this deformation regime are not well understood. Closure of the Mongol-Okhotsk ocean and the ensuing Mongol-Okhotsk orogeny (~140–110 Ma) (Kravchinsky et al., 2002; Cogné et al., 2005) to the East of our study area may have reactivated old fault systems and consequently induced Mesozoic intracontinental deformation in the Altai crust (Novikov, 2002; De Grave et al., 2009). Alternatively, the Cretaceous deformation in Altai can be a far-field response to Cimmerian collisions at the Mesozoic southern Eurasian margin (De Grave et al., 2007).

The thermal history models show that cooling slowed down from about ~90 Ma onwards in the Kalba–Narym terrane (Fig. 5). The ensuing slow cooling of basement rocks corresponds to a Late Mesozoic–Early Cenozoic period of tectonic quiescence and peneplanation in large swaths of the entire CAOB (Dobretsov et al., 1996; Cunningham, 2001). During this time, the intrusives remained approximately at the depth that they had reached after Mesozoic denudation or they slowly cooled further to ambient temperatures at their outcrop position.

The thermal history model for sample KZ-18 seems to exhibit a third, subsequent Neogene fast cooling step (from ~25 Ma onwards). Although the significance of this accelerated cooling step is debatable (Ketcham et al., 1999), it is not observed in other thermal history models and might indicate a renewed period of reactivation along the ISZ. Cenozoic Altai uplift is first recorded in the Eocene (South Altai phase, 40–35 Ma) with increased tectonic activity in the middle Oligocene (Narym phase, 30–25 Ma) and in the late Miocene–Pliocene (Tarbagatai phase, 6–4 Ma) as a response to subsidence of the Zaysan basin (Borisov, 1963; Zykin, 1996). In the intramontane basins of the Mongolian Altai, an Oligocene unconformity marks the onset of deformation (Cunningham, 2001). In the Northern Junggar basin, accelerated subsidence and sediment accumulation is recorded during the Eocene–Oligocene and from the Pleistocene onwards (Chen et al., 2011). These observations testify that a Late Cenozoic Altai orogen was initially built during the Oligocene, which corresponds to the timing of the increase in cooling rate, exhibited by the thermal history model for sample KZ-18. As mentioned earlier (sample descriptions), samples KZ-06 and KZ-18 were taken from clearly sheared granites along the ISZ, while sample KZ-23 and KZ-36 were sampled in the Kalba–Narym batholith, further south of the shear zone, where no shear textures were observed. This observation might explain why only the model for sample KZ-18 exhibits increased cooling in the Late Cenozoic. Hence, the cooling signal might be a result of differential movements during a Late Cenozoic period of intensified shear.

The driving forces that triggered the Cenozoic NW-migration of the Junggar microplate and the subsequent subsidence of the Junggar basin are again open to debate but they can be related to India-Eurasia convergence at the southern Eurasian margin (De Grave et al., 2007) and block reorganization within the CAOB edifice.

4.3. Fault kinematics and tectonic stress reconstructions

The obtained stress inversion results constrain a three-step kinematic evolution for the ISZ fault (Figs. 7 and 8). The ductile fabric of the ISZ is indicative of a marked crustal-scale subvertical heterogeneity, with an ENE-WSW orientation. The first brittle palaeostress stage is observed in granitoids associated with the ISZ in the form of fault planes and tectonic breccias which are often affected by chlorite-epidote metasomatism. This specific type of fault-rock interaction is known to develop as a result of intense brittle shearing, brecciation, high fluid flow and water–rock hydrothermal alteration at temperatures between ~200 and ~400 °C (Axen, 1992; Tomita et al., 2002). These brittle stage structures can be related to detachment faulting connected to deeper mylonitic zones (Axen, 1992). They can also appear as exhumed seismogenic zones (Fujimoto et al., 2002) or even occur in fossil oceanic high-temperature fault-hosted hydrothermal vents (Barker et al., 2010). In this case, we favour the hypothesis that the 'early brittle' stage reflects deep brittle conditions in the granitoids that may even be contemporaneous with the ductile shear displacements along the ISZ itself.

Fractures associated with the 'late brittle' stage are well preserved in the Kalba–Narym granitoids and also affect the ductile fabric of the ISZ. We propose that these were produced by a similar type of stress field as those related to the early brittle stage. The S_{Hmax} orientation for the late brittle stage is however rotated anticlockwise to an orthogonal direction relative to the fabric of the ISZ and indicates a slightly more compressional regime. This could cor-

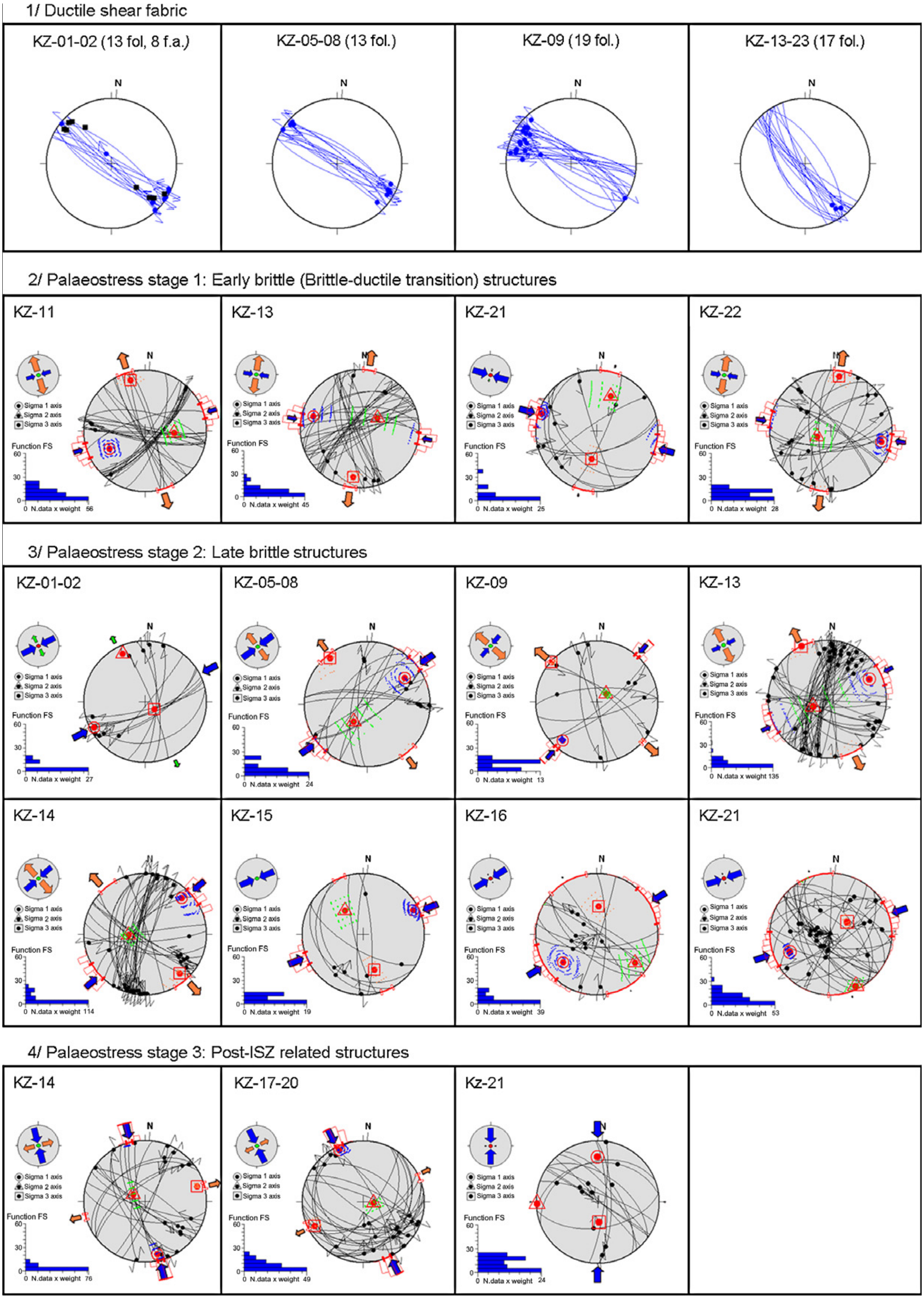

Fig. 7. Fault-slip data and stress inversion. Lower-hemisphere Schmidt stereoplot of the fault-slip data subsets and corresponding stress tensor. Stress symbols show the horizontal stress axes (S_{Hmax} and S_{Hmin}) in function of the stress ratio R. Their length and colour symbolise the horizontal deviatoric stress magnitude, relative to the isotropic stress σ_i. Orange outward arrows: σ_3 stress axis, green arrows: σ_2 stress axis (outward when extensional $\sigma_2 > \sigma_i$) and inward when compressional $\sigma_2 > \sigma_i$), blue inward arrows: σ_1 axis. The vertical stress σ_v is symbolised by a solid circle, orange for extensional regimes $\sigma_1 \sim \sigma_v$), green for strike-slip regimes $\sigma_2 \sim \sigma_v$) or blue for compressional regimes $\sigma_3 \sim \sigma_v$). The histogram represents the distribution of the weighted misfit function. The uncertainties related to the stress axis determination are plotted as small dots (blue for σ_1, green for σ_2, orange for σ_3), and the distribution of possible S_{Hmax} orientations is shown on the outer margin of the net, with 5° frequency interval (bars) and 1σ confidence region (bold red line). fol. = foliations, f.a. = fold axes.

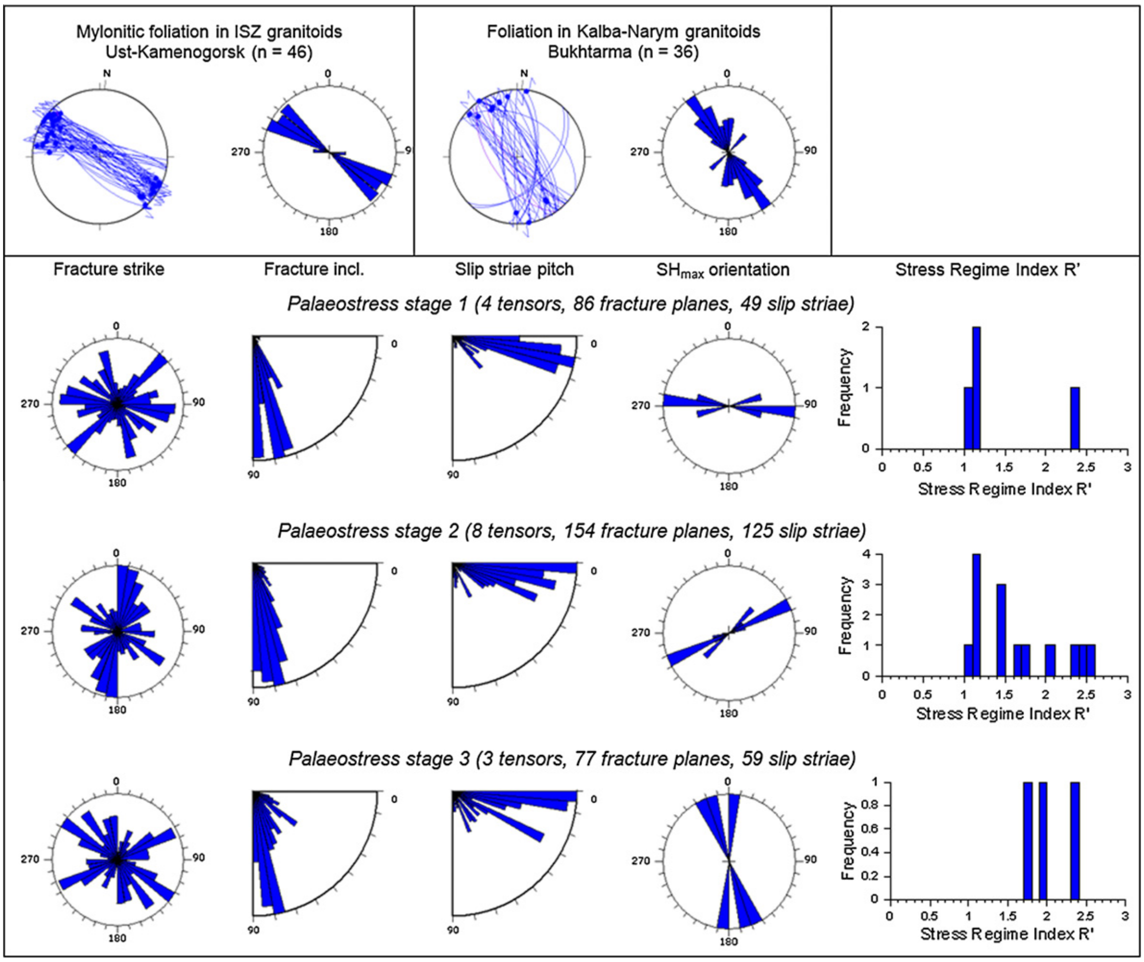

Fig. 8. Synthesis of ductile fabric and fault-slip data subsets with related stress tensors.

respond to late transcurrent displacements along the ISZ, after the cessation of ductile shearing. The reorientation of the S_{Hmax} tensor at a higher angle to the ISZ and the change towards a more compressional regime probably reflects rheological strengthening. The resulting more rigid lithosphere along the ISZ is not surprising, given the cessation of ductile shearing, intensive granitoid emplacement and subsequent cooling of the crust at that time. As shown in an extensional context by Morley (2010), S_{Hmax} trajectories effectively tend to deflect towards parallelism with a relatively weak vertical rock body and they align perpendicular to zones of relatively rigid material. For continental transforms at their early stage of evolution, displacement is commonly distributed over a wide zone (Platt et al., 2008). In the case of the Irtysh shear zone, the large size of the central ductile shear zone and its close association with the granitoids bears witness that if formed within a locally hot crust.

In a later stage, the crust cooled down and deformation became more brittle, focusing on narrow zones that were kept weak due to the presence of fluids. The frequent observation of chlorite-epidote metasomatism along the brittle fault planes, the presence of large base-metal mineralized bodies along the Irtysh shear zone and the widespread magmatic intrusions are clear indicators for high fluid flow in the principal displacement zone. Hence, as for the present-day lithospheric stress along the San-Andreas fault system (Zoback et al., 1987), the horizontal principal compression could have been re-oriented at a high-angle to fault zones that are characterized by very low shear strength. This could explain the apparent anticlockwise rotation of the S_{Hmax} orientations with time, at the vicinity of the shear zone (near-field stress). In addition, a change in regional far-field stress as a response to a slightly more convergent relative movement between the two fault planes could have happened. This can however not be demonstrated with the data presented here.

The final brittle stage that was observed postdates ISZ related displacements and is compatible with the main (Late Plio-Pleistocene) phase of mountain building in the Altai (De Grave et al., 2009; Chen et al., 2011). The faults observed in the Narym range correspond to Late Cenozoic northward thrusting along the southern Altai belt. Along the ISZ however, a discrete and focused dextral strike-slip reactivation was observed which took place under shallow brittle conditions (unconsolidated breccias, iron-oxide coating). The transpressional regime and NNW–SSE to N–S direction of S_{Hmax} correspond to existing palaeostress results for the Chuya depression (Delvaux et al., 1995) and Lake Teletskoye (Dehandschutter et al., 2002) further north in the Siberian Altai.

5. Conclusions

Based on the chronology and palaeostress data-sets, presented in this work, the following conclusions can be drawn regarding the tectonic history of the ISZ with emphasis on its formation and reactivation episodes:

(1) Carboniferous (~338 Ma and ~320 Ma) zircon U/Pb ages, obtained for the syn- and post-collisional Kalba–Narym intrusives along the edge of the ISZ were interpreted in the

framework of the final collision of Siberia with Kazakhstan. The occurrence of older, discordant zircons indicate a limited recycling of Meso-Proterozoic Kazakhstan microcontinental basement during the granitoid emplacement. During or shortly after this period, the ISZ experienced an 'early brittle' left-lateral, mainly transtensional stress regime, reflecting shear conditions with deep lithospheric roots towards the ductile–brittle transition zone.

(2) In several locations along the ISZ, a 'late-brittle', more compressional palaeostress regime was recognized. This change in fault kinematics probably indicates that the ISZ crust underwent rheological strengthening as a response to cessation of ductile shearing, intensive granitoid emplacement and subsequent cooling of the crust. These conditions reflect the geodynamic environment of the ISZ during the Late Palaeozoic–Early Mesozoic.

(3) Late Cretaceous (~100–70 Ma) apatite fission track ages and thermal history modeling results record fast cooling of the ISZ basement as a response to increased denudation of a Mesozoic intracontinental Altai orogen. This mountainous topography was built on the pre-existing structural fabric and is possibly a far-field effect of the Mongol–Okhotsk orogeny.

(4) After a Late Mesozoic–Early Cenozoic period of tectonic quiescence and peneplanation, a renewed cooling signal could be recognized in the thermal history modeling results for the sheared granite sample KZ-18. This signal can be interpreted as a response to increased tectonic activity from the Late Oligocene (~25 Ma) onwards, initiating the present Altai orogeny. A minor transpressional, right-lateral palaeostress stage was observed which is compatible to the main (Late Plio-Pleistocene) phase of mountain building in the Altai along the ISZ. This stage was observed as discrete and focused dextral strike-slip reactivation which took place under shallow brittle conditions.

Acknowledgements

The authors were supported by grants of the Institute for the Promotion of Innovation through Science and Technology in Flanders (IWT-Vlaanderen) (SG) and the Fund for Scientific Research – Flanders (FWO, Belgium) (JDG). This research was also co-funded by Ghent University (BOF – bilateral project 01SB1309). We acknowledge C. Xu and an anonymous reviewer for their insightful comments. A. Fournier-Carrier and A. Izmer are thanked for assistance during sample preparation and LA-ICP-MS measurements respectively. We are indebted to Dr. G. Vittiglio and Dr. P. Vermaercke for help with irradiations and neutron dosimetry at the Belgian Nuclear Research Centre in Mol (SCK–CEN, BR1 facility).

References

Allen, M.B., Vincent, S.J., 1997. Fault reactivation in the Junggar region, northwest China: the role of basement structures during Mesozoic-Cenozoic compression. Journal of the Geological Society 154, 151–155.

Allen, M.B., Sengor, A.M.C., Natalin, B.A., 1995. Junggar, Turfan and Alakol Basins as Late Permian to Early Triassic extensional structures in a sinistral shear zone in the Altaid Orogenic Collage, Central-Asia. Journal of the Geological Society 152, 327–338.

Angelier, J., 1989. From orientation to magnitudes in paleostress determinations using fault slip data. Journal of Structural Geology 11 (1–2), 37–50.

Angelier, J., 1994. Fault slip analysis and paleostress reconstruction. In: Hancock, P.L. (Ed.), Continental Deformation. Pergamon, Oxford, pp. 101–120.

Axen, G.J., 1992. Pore pressure, stress increase, and fault weakening in low-angle normal faulting. Journal of Geophysical Research-Solid Earth 97 (B6), 8979–8991.

Barker, A.K., Coogan, L.A., Gillis, K.M., Hayman, N.W., Weis, D., 2010. Direct observation of a fossil high-temperature, fault-hosted, hydrothermal upflow zone in crust formed at the East Pacific Rise. Geology 38 (4), 379–382.

Borisov, B.A., 1963. Upper Cretaceous and Paleogene–Neogene stratigraphy of the Zaisan depression. In: Borovikov, L.I. (Ed.), Materials on Geology and Useful Minerals of Altay and Kazakhstan. VSEGEI, Leningrad, pp. 11–75.

Bott, M.H.P., 1959. The mechanisms of oblique slip faulting. Geological Magazine 96, 109–117.

Briggs, S.M., Yin, A., Manning, C.E., Chen, Z.L., Wang, X.F., Grove, M., 2007. Late paleozoic tectonic history of the ertix fault in the chinese altai and its implications for the development of the central Asian orogenic system. Geological Society of America Bulletin 119 (7–8), 944–960.

Burtman, V.S., Gugary, G.Z., Belenky, A.V., Kudasheva, I.A., 1998. Kazakhstan and Altai in the Devonian: implications from paleomagnetic data. Geotektonika, 6(63–71).

Buslov, M.M., 2011. Tectonics and geodynamics of the Central Asian foldbelt: the role of the Late Paleozoic large-amplitude strike-slip faults. Russian Geology and Geophysics 52, 66–90.

Buslov, M.M., Saphonova, I.Y., Watanabe, T., Obut, O.T., Fujiwara, Y., Iwata, K., Semakov, N.N., Sugai, Y., Smirnova, L.V., Kazanskii, A.Y., 2001. Evolution of the Paleo-Asian Ocean (Altai-Sayan Region, Central Asia) and collision of possible Gondwana-derived terranes with the southern marginal part of the Siberian continent. Geosciences Journal 5 (3), 203–224.

Buslov, M.M., Watanabe, T., Fujiwara, Y., Iwata, K., Smirnova, L.V., Safonova, I.Y., Semakov, N.N., Kiryanova, A.P., 2004. Late Paleozoic faults of the Altai region, Central Asia: tectonic pattern and model of formation. Journal of Asian Earth Sciences 23 (5), 655–671.

Chen, J.F., Han, B.F., Ji, J.Q., Zhang, L., Xu, Z., He, G.Q., Wang, T., 2010. Zircon U–Pb ages and tectonic implications of Paleozoic plutons in northern West Junggar, North Xinjiang, China. Lithos 115 (1–4), 137–152.

Chen, Z.L., Liu, J.A., Gong, H.L., Han, F.B., Briggs, S.M., Zheng, E.J., Wang, G., 2011. Late Cenozoic tectonic activity and its significance in the Northern Junggar Basin, Northwestern China. Tectonophysics 497 (1–4), 45–56.

Cherniak, D., Watson, E., 2003. Diffusion in zircon. In: Hanchar, J., Hoskin, P. (Eds.), Zircon, pp. 113–139.

Chikov, B.M., Zinoviev, S.V., 1996. Post-Hercynian collisional structures of Western Altai. Russian Geology and Geophysics 37 (11), 59–67.

Chikov, B.M., Zinoviev, S.V., Deyev, E.V., 2008. Mesozoic and Cenozoic collisional structures of the southern Great Altai. Russian Geology and Geophysics 49 (5), 323–331.

Cogné, J.P., Kravchinsky, V.A., Halim, N., Hankard, F., 2005. Late Jurassic–Early Cretaceous closure of the Mongol-Okhotsk Ocean demonstrated by new Mesozoic palaeomagnetic results from the Trans-Baikal area (SE Siberia). Geophysical Journal International 163 (2), 813–832.

Cunningham, W.D., 2001. Cenozoic normal faulting and regional doming in the southern Hangay region, Central Mongolia: implications for the origin of the Baikal rift province. Tectonophysics 331 (4), 389–411.

Cunningham, W.D., Windley, B.F., Dorjnamjaa, D., Badamgarov, G., Saandar, M., 1996. A structural transect across the Mongolian Western Altai: active transpressional mountain building in central Asia. Tectonics 15 (1), 142–156.

De Grave, J., Van den haute, P., 2002. Denudation and cooling of the Lake Teletskoye Region in the Altai Mountains (South Siberia) as revealed by apatite fission-track thermochronology. Tectonophysics 349 (1–4), 145–159.

De Grave, J., Buslov, M.M., Van den Haute, P., 2007. Distant effects of India–Eurasia convergence and Mesozoic intracontinental deformation in Central Asia: constraints from apatite fission-track thermochronology. Journal of Asian Earth Sciences 29 (2–3), 188–204.

De Grave, J., Van den Haute, P., Buslov, M.M., Dehandschutter, B., Glorie, S., 2008. Apatite fission-track thermochronology applied to the Chulyshman Plateau, Siberian Altai Region. Radiation Measurements 43 (1), 38–42.

De Grave, J., Buslov, M.M., Van den haute, P., Metcalf, J., Dehandschutter, B., McWilliams, M.O., 2009. Multi-method chronometry of the Teletskoye graben and its basement, Siberian Altai Mountains: new insights on its thermo-tectonic evolution. In: Lisker, F., Ventura, B., Glasmacher, U.A. (Eds.), Thermochronological Methods: From Palaeotemperature Constraints to Landscape Evolution Models, Geological Society, Special Publications, London, pp. 237–259.

De Grave, J., Glorie, S., Buslov, M.M., Izmer, A., Fournier-Carrie, A., Batalev, V.Y., Vanhaecke, F., Elburg, M.A., Van den haute, P., 2011. The thermo-tectonic history of the Song-Kul plateau, Kyrgyz Tien Shan: constraints by apatite and titanite thermochronometry and zircon U/Pb dating. Gondwana Research 20 (4), 745–763.

Dehandschutter, B., Vysotsky, E., Delvaux, D., Klerkx, J., Buslov, M.M., Seleznev, V.S., De Batist, M., 2002. Kinematic evolution of the Teletsk graben. In: Delvaux, D., De Batist, M., Dobretsov, N.L., Klerkx, J. (Eds.), Tectonic Control of Continental Sedimentary Basins in Altai-Baikal, Central Asia Tectonophysics, pp. 139–168.

Delvaux, D. 2011. The Win-Tensor Program, Version 3.0 and Above. <http://users.skynet.be/damien.delvaux/Tensor/tensor-index.html>.

Delvaux, D., Sperner, B., 2003. Stress tensor inversion from fault kinematic indicators and focal mechanism data: the TENSOR program. In: Nieuwland, D. (Ed.), New Insights into Structural Interpretation and Modelling. Geological Society, Special Publications, London, pp. 75–100.

Delvaux, D., Theunissen, K., Van der Meer, R., Berzin, N.A., 1995. Dynamics and paleostress of the Cenozoic Kurai-Chuya depression of Gorny Altai (South Siberia): tectonic and climatic control. Russian Geology and Geophysics 36 (10), 26–45.

Delvaux, D., Matton, C., Hendriks, B., Buslov, M.M., Erkimov, V., Saphonova, I.Y., Kozlov, M., Bodner, S., 1996. Tectonics and Kinematics of the Irtysh Shear Zone and Zaisan Depression, East Kazakhstan, Continental Rift Basins. Preliminary Results of the Field Season 1996 in Siberia.

Delvaux, D., Moeys, R., Stapel, G., Petit, C., Levi, K., Miroshnichenko, A., Ruzhich, V., San'kov, V., 1997. Paleostress reconstructions and geodynamics of the Baikal region, Central Asia, part 2. Cenozoic rifting. Tectonophysics 282 (1–4), 1–38.

Demoux, A., Kroner, A., Liu, D.Y., Badarch, G., 2009. Precambrian crystalline basement in southern Mongolia as revealed by SHRIMP zircon dating. International Journal of Earth Sciences 98 (6), 1365–1380.

Dobretsov, N.L., Buslov, M.M., Delvaux, D., Berzin, N.A., Ermikov, V.D., 1996. Meso- and Ceno-zoic tectonics of the Central Asian mountain belt: effects of lithospheric plate interaction and mantle plumes. International Geology Review 40, 430–466.

Dokukina, K.A., Konilov, A.N., Kaulina, T.V., Vladimirov, V.G., 2010. Interaction between mafic and felsic magmas in subvolcanic environment (Tastau igneous complex, eastern Kazakhstan). Russian Geology and Geophysics 51 (6), 625–643.

Donelick, R.A., Ketcham, R.A., Carlson, W.D., 1999. Variability of apatite fission-track annealing kinetics: II. Crystallographic orientation effects. American Mineralogist 84 (9), 1224–1234.

Dunkl, I., Mikes, T., Frei, D., Gerdes, A., von Eynatten, H., 2009. PepiAGE: Data Reduction Program for Time-Resolved U/Pb Analyses – Introduction and Call for Tests and Discussion. University of Goettingen Publication, 15pp.

Fujimoto, K., Ohtani, T., Shigematsu, N., Miyashita, Y., Tomita, T., Tanaka, H., Omura, K., Kobayashi, Y., 2002. Water-rock interaction observed in the brittle-plastic transition zone. Earth Planets and Space 54 (11), 1127–1132.

Glorie, S., De Grave, J., Buslov, M.M., Elburg, M.A., Stockli, D.F., Gerdes, A., Van den Haute, P., 2010. Multi-method chronometric constraints on the evolution of the Northern Kyrgyz Tien Shan granitoids (Central Asian Orogenic Belt): from emplacement to exhumation. Journal of Asian Earth Sciences 38 (3–4), 131–146.

Glorie, S., De Grave, J., Buslov, M.M., Zhimulev, F.I., Stockli, D.F., Batalev, V.Y., Izmer, A., Van den haute, P., Vanhaecke, F., Elburg, M.A., 2011a. Tectonic history of the Kyrgyz South Tien Shan (Atbashi–Inylchek) suture zone: the role of inherited structures during deformation-propagation. Tectonics. doi:10.1029/2011TC002949.

Glorie, S., De Grave, J., Buslov, M.M., Zhimulev, F.I., Izmer, A., Vandoorne, W., Ryabinin, A., Van den Haute, P., Vanhaecke, F., Elburg, M.A., 2011b. Formation and Palaeozoic evolution of the Gorny-Altai – Altai-Mongolia suture zone (South Siberia): zircon U/Pb constraints on the igneous record. Gondwana Research 20 (2–3), 465–484.

Jackson, S.E., Pearson, N.J., Griffin, W.L., Belousova, E.A., 2004. The application of laser ablation-inductively coupled plasma-mass spectrometry to in situ U–Pb zircon geochronology. Chemical Geology 211 (1–2), 47–69.

Jahn, B.M., 2004. The central Asian orogenic belt and growth of the continental crust in the phanerozoic. Journal of the Geological Society 226, 73–100.

Jolivet, M., Ritz, J.F., Vassallo, R., Larroque, C., Braucher, R., Todbileg, M., Chauvet, A., Sue, C., Arnaud, N., De Vicente, R., Arzhanikova, A., Arzhanikov, S., 2007. Mongolian summits: an uplifted, flat, old but still preserved erosion surface. Geology 35 (10), 871–874.

Jolivet, M., Arzhannikova, A., Arzhannikov, S., Vassallo, R., Chauvet, A., 2011. Pliocene to Quaternary deformation in South East Sayan (Siberia): initiation of the tertiary compressive phase in the southern termination of the Baikal Rift System. Journal of Asian Earth Sciences 40 (2), 581–594.

Ketcham, R.A., 2005. Forward and inverse modelling of low-temperature thermochronometry data. Reviews in Mineralogy and Geochemistry 58, 275–314.

Ketcham, R.A., Donelick, R.A., Carlson, W.D., 1999. Variability of apatite fission-track annealing kinetics: III. Extrapolation to geological time scales. American Mineralogist 84 (9), 1235–1255.

Khromykh, S.V., Kuibida, M.L., Kruk, N.N., 2011. Petrogenesis of high-temperature siliceous melts in volcanic structures of the Altai collisional system of Hercynides (Eastern Kazakhstan). Russian Geology and Geophysics 52 (4), 411–420.

Kozakov, I.K., Kotov, A.B., Sal'nikova, E.B., Bibikova, E.V., Kovach, V.P., Kirnozova, T.I., Berezhnaya, N.G., Lykhin, D.A., 1999. Metamorphic age of crystalline complexes of the Tuva-Mongolia Massif: the U–Pb geochronology of granitoids. Petrology 7 (2), 177–191.

Kravchinsky, V.A., Cogne, J.P., Harbert, W.P., Kuzmin, M.I., 2002. Evolution of the Mongol–Okhotsk Ocean as constrained by new palaeomagnetic data from the Mongol–Okhotsk suture zone, Siberia. Geophysical Journal International 148 (1), 34–57.

Kuibida, M.L., Kruk, N.N., Vladimirov, A.G., Polyanskii, N.V., Nikolaeva, I.V., 2009. U–Pb isotopic age, composition, and sources of the plagiogranites of the Kalba range, Eastern Kazakhstan. Doklady Earth Sciences 424 (1), 72–76.

Ludwig, K., 2003. User's Manual for Isoplot 3.00. A Geochronological Toolkit for Microsoft Excell. Berkely Geochronology Center Special Publication v. 4.

Lund, B., Townend, J., 2007. Calculating horizontal stress orientations with full or partial knowledge of the tectonic stress tensor. Geophysical Journal International 170 (3), 1328–1335.

Melnikov, A., Delvaux, D., Travin, A., Buslov, M.M., Vladimirov, A.G., Vladimirov, V.G., Plotnikov, A., Berzin, N., Smirnova, L., Trefois, P., Theunissen, K., 1997. Late Paleozoic-Early Mesozoic Sinistral Movement along the Irtysh shear zone, NE-Kazakhstan. In: Abstract for the Tectonic Studies Group Annual General Meeting, Durham.

Morley, C.K., 2010. Stress re-orientation along zones of weak fabrics in rifts: an explanation for pure extension in 'oblique' rift segments? Earth and Planetary Science Letters 297 (3–4), 667–673.

Novikov, I.S., 2002. Late Paleozoic, Middle Mesozoic, and Late Cenozoic stages of the Altai orogeny. Geologiya I Geofizika 43 (5), 434–445.

Pirajno, F., 2010. Intracontinental strike-slip faults, associated magmatism, mineral systems and mantle dynamics: examples from NW China and Altay-Sayan (Siberia). Journal of Geodynamics 50 (3–4), 325–346.

Platt, J.P., Kaus, B., Becker, T.W., 2008. The mechanics of continental transforms: an alternative approach with applications to the San-Andreas system and the tectonics of California. Earth and Planetary Science Letters 274 (3–4), 380–391.

Reiners, P.W., Ehlers, T.A., 2005. Low-Temperarture Thermochronology: Techniques, Interpretations, and Applications. Reviews in Mineralogy and Geochemistry, vol. 58. Mineralogical Society of America, Chantilly, Virginia, 622pp.

Şengör, A.M.C., Natalin, B.A., Burtman, V.S., 1993. Evolution of the Altaid Tectonic Collage and Paleozoic Crustal Growth in Eurasia. Nature 364 (6435), 299–307.

Sláma, J., Kosler, J., Condon, D.J., Crowley, J.L., Gerdes, A., Hanchar, J.M., Horstwood, M.S.A., Morris, G.A., Nasdala, L., Norberg, N., Schaltegger, U., Schoene, B., Tubrett, M.N., Whitehouse, M.J., 2008. Plesovice zircon – a new natural reference material for U–Pb and Hf isotopic microanalysis. Chemical Geology 249 (1–2), 1–35.

Thomas, J.C., Lanza, R., Kazansky, A., Zykin, V., Semakov, N., Mitrokhin, D., Delvaux, D., 2002. Paleomagnetic study of Cenozoic sediments from the Zaisan basin (SE Kazakhstan) and the Chuya depression (Siberian Altai): tectonic implications for central Asia. Tectonophysics 351 (1–2), 119–137.

Tomita, T., Ohtani, T., Shigematsu, N., Tanaka, H., Fujimoto, K., Kobayashi, Y., Miyashita, Y., Omura, K., 2002. Development of the Hatagawa Fault Zone clarified by geological and geochronological studies. Earth Planets and Space 54 (11), 1095–1102.

Travin, A.V., Boven, A., Plotnikov, A.V., Vladimirov, V.G., Theunissen, K., Vladimirov, A.G., Melnikov, A.I., Titov, A.V., 2001. Ar-40/Ar-39 dating of ductile deformations in the Irtysh shear zone, eastern Kazakhstan. Geochemistry International 39 (12), 1237–1241.

Vassallo, R., Jolivet, M., Ritz, J.F., Braucher, R., Larroque, C., Sue, C., Todbileg, M., Javkhlanbold, D., 2007. Uplift age and rates of the Gurvan Bogd system (Gobi-Altay) by apatite fission track analysis. Earth and Planetary Science Letters 259 (3–4), 333–346.

Vincent, S.J., Allen, M.B., 2001. Sedimentary record of Mesozoic intracontinental deformation in the eastern Junggar Basin, north-west China: response to orogeny at the Asian margin. In: Hendrix, M.S., Davis, G.A. (Eds.), Palaeozoic and Mesozoic Tectonic Evolution of Central and Eastern Asia: From Continental Assembly to Intracontinental Deformation. Geological Society of America Memoir, pp. 341–360.

Vladimirov, A.G., Kozlov, M.S., Shokal'skii, S.P., Khalilov, V.A., Rudnev, S.N., Kruk, N.N., Vystavnoi, S.A., Borisov, S.M., Berezikov, Y.K., Metsner, A.N., Babin, G.A., Mamlin, A.N., Murzin, O.M., Nazarov, G.V., Makarov, V.A., 2001. Major epochs of instrusive magmatism of Kuznetsk Alatau, Altai, and Kalba (from U–Pb isotope dates). Geologiya I Geofizika 42 (8), 1157–1178.

Vladimirov, A.G., Kruk, N.N., Rudnev, S.N., Khromykh, S.V., 2003. Geodynamics and granitoid magmatism of collision orogens. Geologiya I Geofizika 44 (12), 1321–1338.

Vladimirov, A.G., Kruk, N.N., Khromykh, S.V., Polyansky, O.P., Chervov, V.V., Vladimirov, V.G., Travin, A.V., Babin, G.A., Kuibida, M.L., Khomyakov, V.D., 2008. Permian magmatism and lithospheric deformation in the Altai caused by crustal and mantle thermal processes. Russian Geology and Geophysics 49 (7), 468–479.

Wagner, G.A., Van den haute, P., 1992. Fission Track-Dating. Kluwer Academic Publishers, Dordrecht.

Wallace, R.E., 1951. Geometry of shearing stress and relation to faulting. Journal of Structural Geology 59, 118–130.

Wang, T., Jahn, B.M., Kovach, V.P., Tong, Y., Hong, D.W., Han, B.F., 2009. Nd–Sr isotopic mapping of the Chinese Altai and implications for continental growth in the Central Asian Orogenic Belt. Lithos 110 (1–4), 359–372.

Windley, B.F., Kroner, A., Guo, J.H., Qu, G.S., Li, Y.Y., Zhang, C., 2002. Neoproterozoic to Paleozoic geology of the Altai orogen, NW China: new zircon age data and tectonic evolution. Journal of Geology 110 (6), 719–737.

Windley, B.F., Alexeiev, D., Xiao, W.J., Kroner, A., Badarch, G., 2007. Tectonic models for accretion of the Central Asian Orogenic Belt. Journal of the Geological Society 164, 31–47.

Yuan, W.M., Carter, A., Dong, J.Q., Bao, Z.K., An, Y.C., Guo, Z.J., 2006. Mesozoic-tertiary exhumation history of the Altai Mountains, northern Xinjiang, China: new constraints from apatite fission track data. Tectonophysics 412 (3–4), 183–193.

Yuan, C., Sun, M., Xiao, W., Li, X., Chen, H., Lin, S., Xia, X., Long, X., 2007. Accretionary orogenesis of the Chinese Altai: insights from Paleozoic granitoids. Chemical Geology 242 (1–2), 22–39.

Yuan, W.M., Zheng, Q.G., Bao, Z.K., Dong, J.Q., Carter, A., An, Y.C., Deng, J., 2009. Zircon fission track thermochronology constraints on mineralization epochs in Altai Mountains, northern Xinjiang, China. Radiation Measurements 44 (9–10), 950–954.

Yuan, C., Sun, M., Wilde, S., Xiao, W.J., Xu, Y.G., Long, X.P., Zhao, G.C., 2010. Post-collisional plutons in the Balikun area, East Chinese Tianshan: evolving magmatism in response to extension and slab break-off. Lithos 119 (3–4), 269–288.

Zoback, M.D., Zoback, M.L., Mount, V.S., Suppe, J., Eaton, J.P., Healy, J.H., Oppenheimer, D., Reasenberg, P., Jones, L., Raleigh, C.B., Wong, I.G., Scotti, O., Wenworth, C., 1987. New evidence on the state of stress of the San Andreas fault system. Science 238 (4830), 1105–1111.

Zykin, V.S., 1996. Upper Cretaceous and Cenozoic Stratigraphy of the Zaisan Depression, Continental Rift Basins. Preliminary Results of the Field Season 1996 in Siberia.